Heliyon 8 (2022) e10862

Contents lists available at ScienceDirect

Heliyon

journal homepage: www.cell.com/heliyon

Research article

# Claudin-4 localization in epithelial ovarian cancer

Margaret C. Neville [a,*], Patricia G. Webb [b], Heidi K. Baumgartner [c], Benjamin G. Bitler [d]

[a] Departments of Obstetrics and Gynecology and Physiology and Biophysics, University of Colorado School of Medicine, Aurora, CO, 80845, USA
[b] Department of Obstetrics and Gynecology, University of Colorado School of Medicine, Aurora, CO, 80845, USA
[c] University of Colorado Anschutz Medical Campus, 2700 E. 19th Ave., Aurora, CO, 80045, USA
[d] Department of Obstetrics and Gynecology, Division of Reproductive Sciences, University of Colorado Denver Anschutz Medical Campus, Mail Stop 8613, 12700 E. 19th Ave., Aurora, CO, 80045, USA

ARTICLE INFO

*Keywords:*
Claudin-4
Ovarian cancer
Golgi
Endoplasmic reticulum
Endosome
Cell-cell contacts
Plasma membrane proteins
Cell architecture

ABSTRACT

Claudin-4, a protein with the structure of classic claudins most often found in cell-cell junctions, is frequently overexpressed in epithelial cancers where its localization has not been studied. In this study we aimed to find out where this membrane protein is localized in an ovarian tumor model, OVCAR3 cells, that express high levels of the protein. Immunohistochemical studies showed claudin-4 staining in a perinuclear region, at most plasma membranes and in cytoplasmic puncta. Native claudin-4 did not overlap with phosphorylated claudin-4, which was partially located in focal adhesions. Using claudin-4 BioID technology we confirmed that large amounts of claudin-4 are localized to the Golgi compartment, including in dispersed Golgi in cells where claudin-4 is partially knocked down and in dividing cells. Claudin-4 appears to be present in the vicinity of several types of cell-cell junctions, but there is no evidence that it forms tight junctions in these tumor cells. Both claudin-4, the Golgi marker GM130, and the plasma membrane receptor Notch2 were found in dispersed Golgi in dividing cells. This definition of the cellular architecture of claudin-4 should provide a framework for better understanding of the function of claudin-4 in tumor cells and its molecular interactions.

## 1. Introduction

High grade serous ovarian cancer (HGSOC) is the most lethal of the tumors of the female reproductive system. In 2022, it is estimated that nearly 20,000 individuals will be newly diagnosed with this cancer and nearly 13,000 will die of the disease (ACS, 2022). Claudin-4 (protein)/*CLDN4* (RNA) was identified more than two decades ago as a frequently overexpressed gene in ovarian cancer (Hough et al., 2000). In cultured cells, such as MDCK kidney cells and EPH4 mammary cells, claudin-4 localizes to tight junctions and contributes to transcellular resistance (Baumgartner et al., 2011; Fredriksson et al., 2015). Although claudin-4 is found in a number of normal tissues including bladder, salivary glands (Zhang et al., 2018b) gastrointestinal tract (Schumann et al., 2012), and kidney (Gong and Hou, 2017), it is not entirely clear that it normally functions as a tight junction protein (Piontek et al., 2020). It is also found in damaged lung cells (Schlingmann et al., 2015) and in epithelial cells of the involuting, but not the milk-secreting, mammary gland (Baumgartner et al., 2017). Claudin-4 is often overexpressed in epithelial cancers (Hewitt et al., 2006) including breast (Kolokytha et al., 2014; Szasz et al., 2011), prostate (Landers et al., 2008; Li, 2021), gastric (Soini et al., 2006; Liu and Li, 2020), pancreatic (Li, 2021; Torres et al., 2018), bladder (Kuwada et al., 2015), lung (Li, 2021), colorectal (Fujiwara-Tani et al., 2018; Holczbauer et al., 2013) and ovarian (Hewitt et al., 2006; Hough et al., 2000; Li, 2021). Survival time in ovarian cancer patients is decreased when tumors have high levels of claudin-4 (Yoshida et al., 2011; Martin de la Fuente et al., 2018). Knockdown of claudin-4 has recently been found to sensitize ovarian cancer cells to paclitaxel and PARP inhibitors (Breed et al., 2019; Yamamoto et al., 2022) and targeting of claudin-3 and claudin-4 has been proposed as a chemotherapeutic strategy in ovarian cancer (Uthayanan and El-Bahrawy, 2022). In order to better understand the biology of claudin-4 in epithelial cancers it is necessary to know its localization in tumor cells, particularly since it is not thought to localize to tight junctions.

Claudins are a family of 23 tetraspanin proteins in humans, each with four alpha helixes which cross the plasma membrane separated by two extracellular loops and a short intracellular loop (Figure 1A). The extracellular loops are hydrophobic and often interact in *trans* with loops of similar molecules on adjacent cells to form tight junctions. Claudin-4 has the general structure of classic claudins (Piontek et al., 2020); the N-terminus is cytoplasmic and short, commencing with a methionine-alanine

* Corresponding author.
*E-mail address:* Peggy.Neville@cuanschutz.edu (M.C. Neville).

https://doi.org/10.1016/j.heliyon.2022.e10862
Received 7 July 2022; Received in revised form 6 September 2022; Accepted 28 September 2022

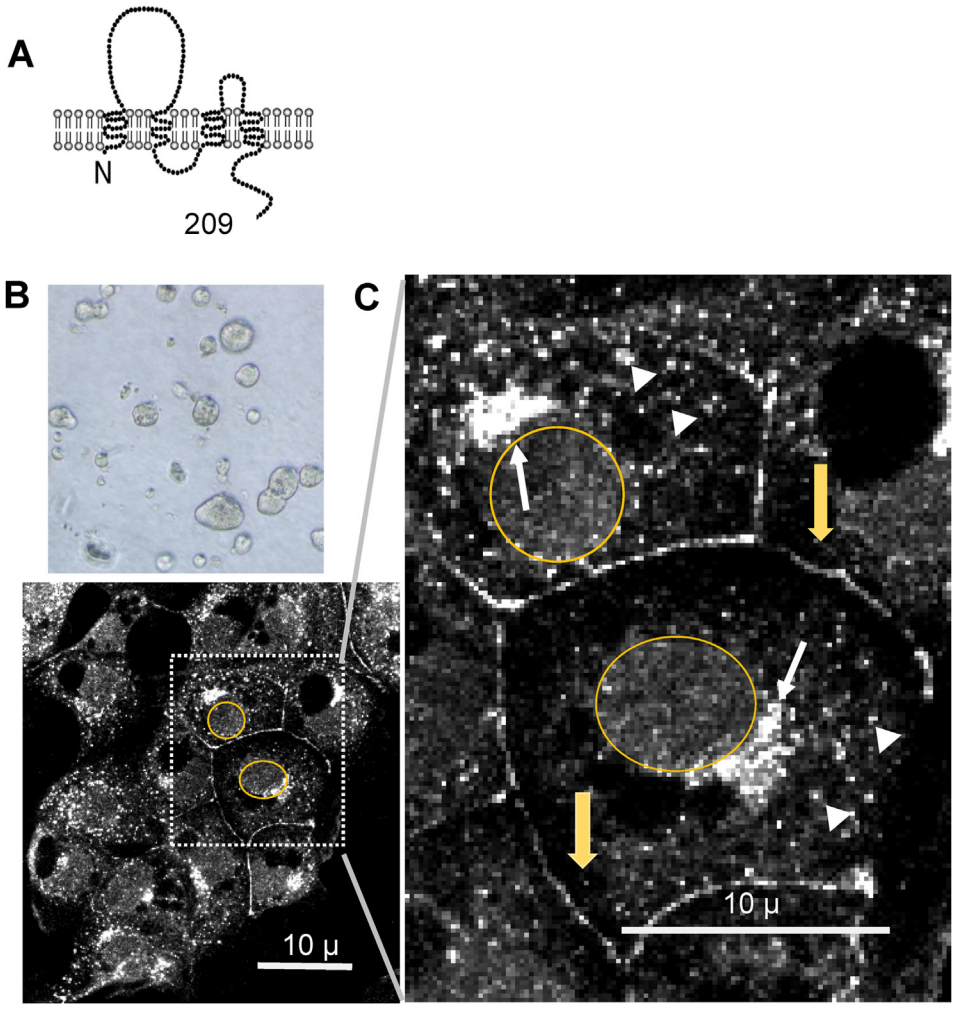


**Figure 1.** A. Cartoon of claudin structure showing a short N-terminus, four transmembrane segments, two extracellular loops and a more extensive carboxy-terminus ending at amino acid 209 in humans (C209). B. A low power view of clusters of OVCAR3 cells grown on collagen. C. Immuno-histochemistry for claudin-4 distribution (white) in a clump of OVCAR3 cells grown on a collagen matrix. Nuclei are circled in gold for clarification of their position. In the magnified image white stained clumps of puncta are localized near the nucleus at the position of Golgi vesicles (white arrows); arrowheads indicate cytoplasmic puncta; yellow arrows indicate cell-cell borders. That claudin-4 localizes near proteins in the membranes of these structures will be shown in the Bio-ID experiments to follow.

sequence. This terminus allows the attachment of biotin ligase for the BioID experiments to be described in this paper. The length of the cytoplasmic carboxy-terminus is variable containing about 27 amino acids depending on species. This segment terminates in the sequence YV as in all classic claudins (Piontek et al., 2020), allowing the membrane molecule to interact with the PDZ domains of submembrane cytoskeletal molecules like ZO1.

Our laboratory has demonstrated that claudin-4 contributes functionally to ovarian tumor cell survival, migration, and overall tumor burden (Hicks et al., 2016). However, the molecular mechanisms involved remain largely unknown. In this paper, we present the results of our studies of claudin-4 localization in an ovarian tumor cell line, OVCAR3, that expresses high levels of claudin-4 compared to most HGSOC cell lines (Breed et al., 2019). We examine control OVCAR3 (OVCAR3-shCTRL) cells and cells in which claudin-4 is partially knocked down (OVCAR3-shCLDN4) as well as OVCAR8 cells, an ovarian cancer cell line that has undetectable levels of claudin-4. We examine the localization of unphosphorylated claudin-4 and claudin-4 phosphorylated on tyrosine residue 208. We then use BioID technology to examine proteins expressed in the vicinity of claudin-4 in order to confirm localization to most membranes of this ovarian cancer cell line as seen in immunocytochemical images.

## 2. Results

**Localization of claudin-4 in OVCAR3 cells.** Claudin-4 has a short N-sequence, four hydrophobic transmembrane segments, two extracellular loops, and a C-terminus with about 22 amino acids ending at amino acid 209 in humans (Figure 1A). Breed and colleagues (Breed et al., 2019) showed by Western blot that OVCAR3 and several other cell lines (PEO4, OV429, and OVCAR5) express high levels of claudin-4 protein, whereas the protein was not visible in Western blots from OVCAR8, OVCAR4, and DOV13 cells. We chose OVCAR3 (claudin-4 positive, Log2 TPM Expression = 7.25) and OVCAR8 (claudin-4 negative, Log2 TPM Expression = 0.94) cell lines for further study. To determine where claudin-4 is localized in OVCAR3 cells, we performed immunocytochemistry using confocal microscopy. We evaluated claudin-4 localization in clumps of OVCAR3 cells grown on a collagen matrix (Figure 1B) using an antibody to the final 22 amino acids of the C-terminus of human claudin-4. A blocking peptide attenuated the signal in OVCAR3 cells verifying the specificity of the antibody used (see Supplementary Material, Figure 1). Figure 1C shows that the claudin-4 in OVCAR3 cells is clustered in puncta near the nucleus (white arrows). Claudin-4 is also found in isolated cytoplasmic puncta (arrowheads) and in the plasma membrane, possibly associated in part with cell-cell junctions (yellow arrows).

**Claudin-4 phosphorylated on tyrosine 208 does not overlap with non-phosphorylated claudin-4.** The C-terminus of claudin-4 has known phosphorylation sites that serve to facilitate claudin-4-protein interactions (Figure 2A). We used an antibody to the C-terminal peptide of claudin-4 with phosphorylated tyrosine 208. Dual staining of OVCAR3 cells with the antibody to claudin-4 and the antibody to p(208)-claudin-4 is shown in Figure 2B. Claudin-4 (non-phosphorylated claudin-4, green) and p(208)-claudin-4 (Y208 phosphorylated, red) did not overlap as shown clearly in the images in Figure 2B. Non-phosphorylated

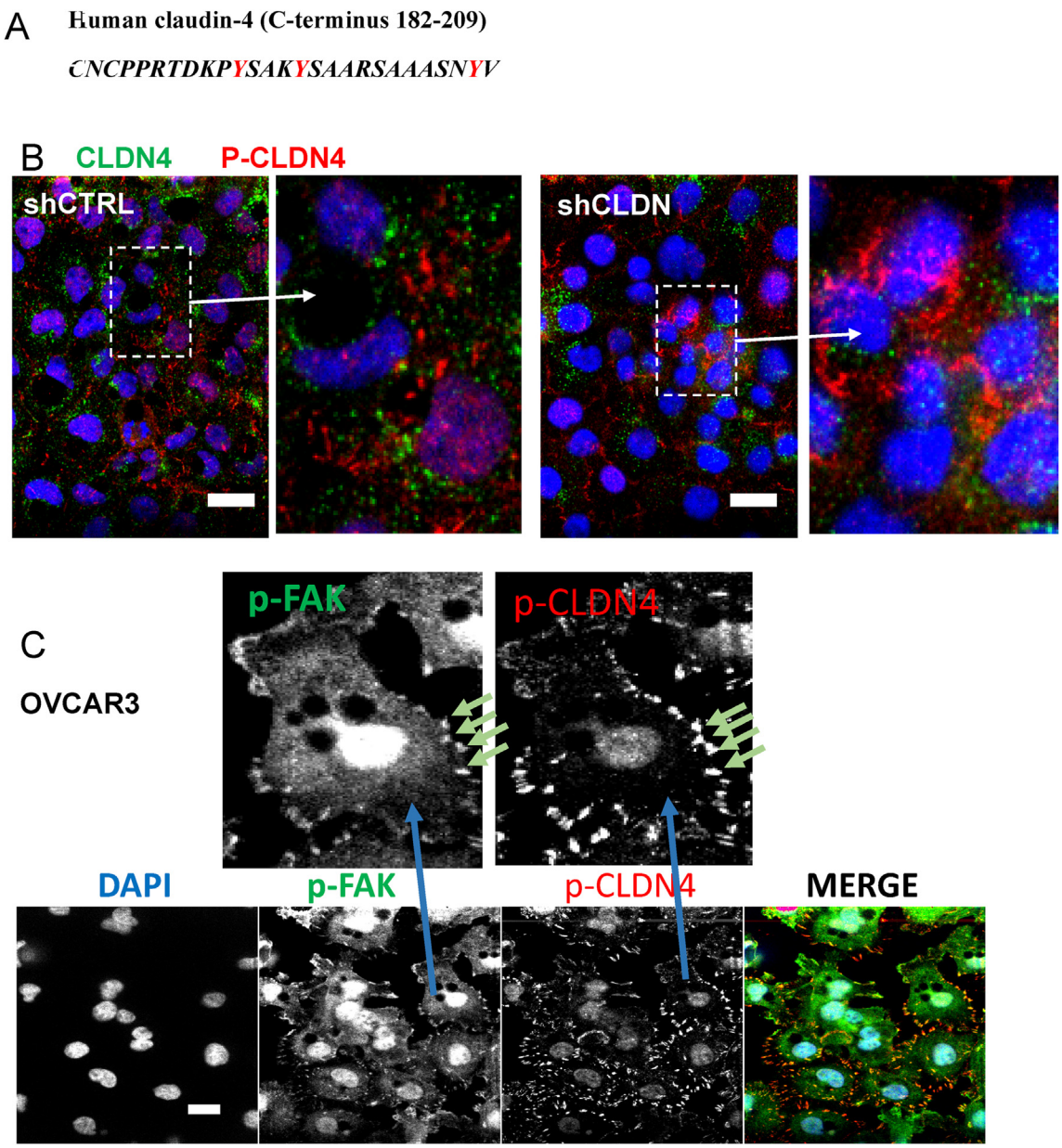


**Figure 2.** Phosphorylated claudin-4 does not overlap with non-phosphorylated claudin-4. A. The c-terminus of human claudin-4 has three tyrosine phosphorylation sites at residues 193, 197, and 208 9 (red) (Van Itallie and Anderson, 2018). B. Distribution of nuclei (DAPI, blue), non-phosphorylated claudin-4 (green), and claudin phosphorylated at Y-208 (red) in OVCAR3 shCTRL and OVCAR3 shCLDN4 cells. C. Three color view of the distribution of phospho-claudin-4 and focal adhesion kinase (FAK) in OVCAR3 shCTRL cells. Green arrows identify puncta of co-localized p(Y397)-FAK and p-CLDN4. Scale bars: 10 μ.

claudin-4 shows clear perinuclear and cytoplasmic puncta. In contrast, the p(208)-CLDN4 stain is confined to puncta distributed closer to the periphery of the cell as well as some nuclear stain indicating that phosphorylation alters the cellular distribution of claudin-4.

There is less claudin-4 stain in the shCLDN4 knockdown cells as expected (the same cell line as shCLDN4_2 in the Breed paper where claudin-4 was shown to be decreased markedly by Western blot in these cells (Supplementary Figure 4 (Breed et al., 2019)). Interestingly, the stain for p(208)-claudin-4 does not appear to be diminished in shCLDN4 cells examined immunohistochemically. To help determine the localization of the p(208)-claudin-4 puncta, we costained OVCAR3 cells with an antibody to pY397 focal-adhesion kinase (pFAK), finding that it stained some cytoplasmic puncta that overlapped with p-claudin-4 (Figure 2C). Focal adhesions assist in cell mobility suggesting a role for p(208)-claudin-4 in cell migration. If non-phosphorylated claudin-4 plays a role in cell mobility it must be by a different mechanism since p(208)-claudin-4 and native claudin-4 do not overlap (Figure 2B).

**Claudin-4 accumulates in the Golgi of OVCAR3 cells.** The perinuclear puncta observed in Figure 1C suggest claudin-4 accumulation in the Golgi complex. We examined claudin-4 co-localization with a known Golgi-specific protein, GM130 (Figure 3A), and found that the two proteins often co-localized (yellow in the merged image) in a perinuclear compartment. As in Figure 1, claudin-4 is also observed in numerous cytoplasmic puncta as well as at cell borders. When claudin-4 was knocked down in shCLDN4 cells, the Golgi became fragmented, as is often seen in cancer cells (Petrosyan, 2015). Very little claudin-4 could be observed by immunohistochemistry, but what was there also appeared to have a fragmented distribution (Figure 3B).

The area occupied by claudin-4 and GM130 was quantitated using Slidebook software. The data in Table 1 show first that the cross-sectional

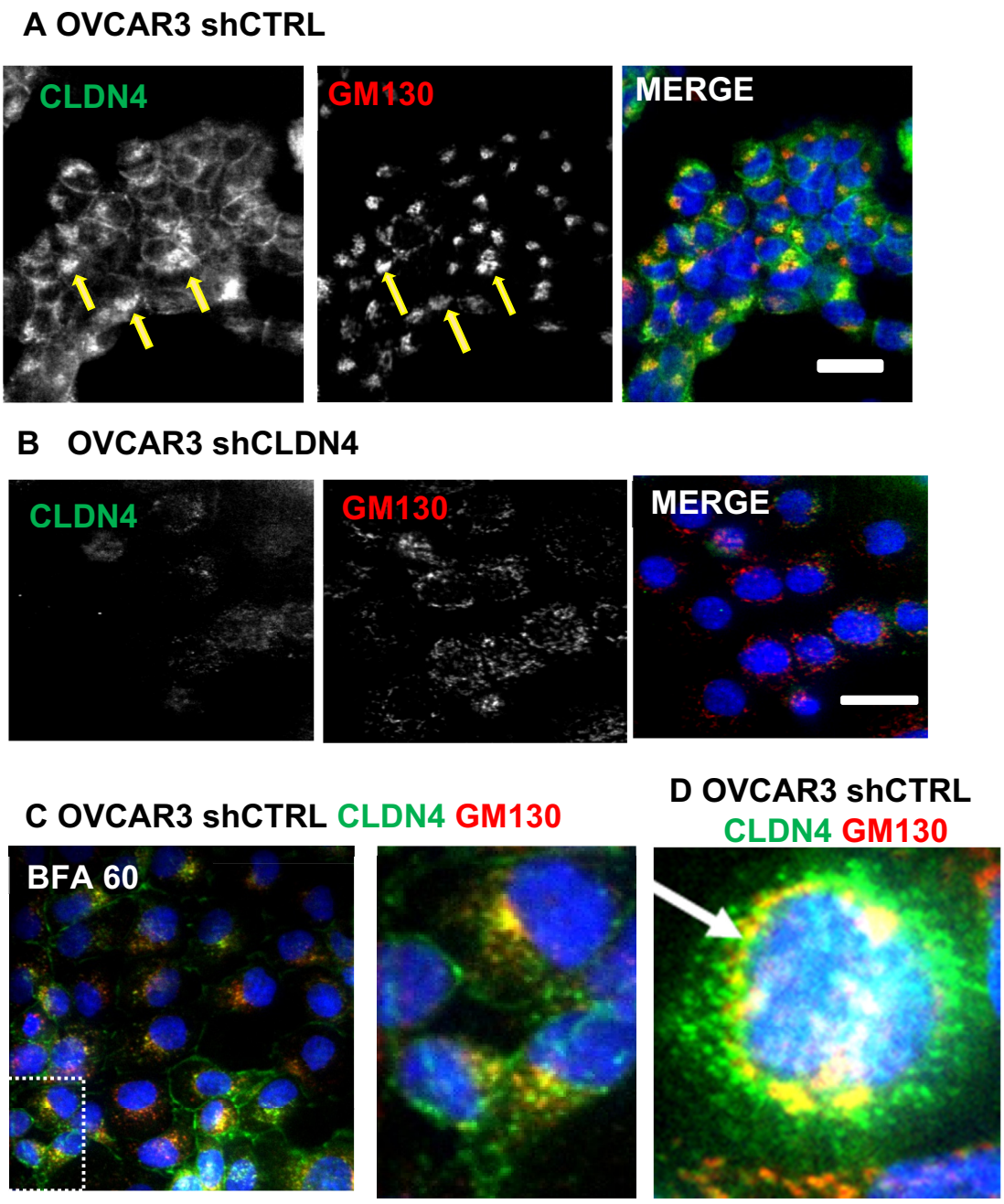


**Figure 3.** Claudin-4 and GM130 colocalization in adherent OVCAR3 cells. A. In OVCAR3 shCTRL cells perinuclear assemblages of stain for CLDN4 (green in merged image) overlap with most of the clusters of stain for the Golgi marker, GM130 (red in the merged image). A few of these overlapping clusters are indicated by the yellow arrows. Nuclei are stained blue (DAPI) in the merged image. B. In the OVCAR3 knockdown shCLDN4 cells, claudin-4 stain is sparse, and Golgi are dispersed as indicated by the GM130 stain in the knockdown cells. See Table 1 for quantitation of the areas occupied by CLDN4 and GM130 in OVCAR3 shCNTL and shCLDN4 cells. C. Effect of Brefeldin A (BFA) on the distribution of CLDN4 (green) and GM130 (red). OVCAR3 control cells were incubated with 10 μg/ml BFA for 60 min then fixed and imaged. The boxed space was enlarged in the figure to the right. D. A dividing cell showing colocalization of the Golgi marker GM130 and claudin-4 in dispersed vesicles near nuclei (white arrow). Scale bars: 10 μM.

area occupied by cells in which claudin-4 is partially knocked down (2328 $\mu^2$) is about double that of the control cells (1270 $\mu^2$). In the knockdown cells claudin-4 occupied an average of 329 $\mu^2$ or about 26% of the total cross-sectional area of the cell, whereas GM130 stain occupied about 79 $\mu^2$ or only about 6% of the total cell area. However, 85% of the area occupied by GM130 also contained claudin-4 indicating that a majority of Golgi vesicles contain claudin-4. When claudin-4 was knocked down with shRNA (cells labelled shCLDN4), claudin-4 occupied 358 $\mu^2$ or only about 16% of the area of these larger cells. The area occupied by the Golgi (GM130 marker) nearly doubled to 140 $\mu^2$ in the shCLDN4 cells, again about 6% of the total area. Although very light in its stain, claudin-4 was still found in about 54% of the fragmented Golgi area. Thus, in both cell types, about 20% of the total claudin-4 protein was associated with the Golgi. These results tell us that claudin-4 has a broad distribution in both shCTRL and shCLDN4 ovarian cancer cells and that the distribution of claudin-4 is not simply a function of the high expression level of this protein in OVCAR3 cells.

**The effect of Brefeldin A on CLDN4 distribution.** Brefeldin A (BFA) is an antiviral lactone first isolated from the fungus *Penicillium Brefeldianum*. It inhibits protein transport from the endoplasmic reticulum to

**Table 1.** Effect of claudin-4 knockdown on cell size and Golgi area.

| Area | Units | shCTRL | shCLDN4 | N | P |
|---|---|---|---|---|---|
| Average total cell area | $u^2$ | 1,270 ± 104 | 2,328 ± 205 | 10 | 0.0001 |
| CLDN4 area per cell | $u^2$/cell | 329 ± 65 | 358 ± 84 | 5 | 0.3987 |
| GM130 area (Golgi) | $u^2$/cell | 79 ± 22 | 140 ± 41 | 5 | 0.1140 |
| CLDN4/GM130 overlap | $u^2$/cell | 67 ± 18 | 76 ± 28 | 5 | 0.3956 |
| **Percent of total cell area** | | | | | |
| CLDN4 area | % cell area | 25.61 ± 4.88 | 15.56 ± 3.81 | 5 | 0.0716 |
| GM130 (Golgi) | % cell area | 6.04 ± 1.65 | 5.90 ± 1.78 | 5 | 0.4785 |
| **Overlap as percent of total cell area** | | | | | |
| %GM130 with CLDN4 | % cell area | 84.81 ± 1.66 | 54.28 ± 6.20 | 5 | 0.0165 |
| %CLDN4 with GM130 | % cell area | 20.36 ± 1.94 | 21.23 ± 6.01 | 5 | 0.1090 |
| | | Mean ± SEM | Mean ± SEM | | |

ShCTRL refers to control cells. shCLDN4 refers to CLDN4 knockdown cells. N is the number of sections analyzed.

the Golgi leading to dissociation of the Golgi stack into dispersed vesicles particularly associated with mitosis (Colanzi et al., 2013). We treated OVCAR3 cells, with 10 μg/ml BFA for 60 min. The dispersion of the Golgi stack observed after 60 min is shown in Figure 3C, where the Golgi marker GM130 is imaged along with claudin-4. These images along with those of shCLDN4 above indicate that fragmentation does not alter the association of claudin-4 with the Golgi vesicles. In dividing cells the Golgi vesicles are dispersed (Figure 3D) but still contain both claudin-4 and GM130.

**Proteins biotinylated by biotin ligase labelled claudin-4 in OVCAR3 and OVCAR8 cells.**

The distribution of claudin-4 shown in Figure 1 suggests that the protein is distributed in many of the membrane components of the cell. To verify this localization, we next determined claudin-4 proximity proteins using BioID technology as described in the methods. Two experiments each were carried out in the OVCAR3 and the OVCAR8 cell lines. OVCAR3 and OVCAR8 cells expressing claudin-4-biotin ligase were cultured on collagen I and incubated with biotin. The proximity of claudin-4-biotin ligase to neighboring proteins (within 10–15 nm) leads to their biotinylation. Biotinylated proteins were purified and identified via mass spectrometry. Because the results differed little between the two cell lines, they were combined giving 52 proteins localized near to the N-terminus of claudin-4 (Supplementary Table 1 and Supplementary Tables 2A to 2G). Two carboxylases, ACACA and ACACB, and a scaffold protein, AHNAK, were also identified. ACACA and ACACB are not considered further in this paper since they are endogenously biotinylated, giving variable results. AHNAK is also heavily biotinylated in controls and didn't meet the criteria for inclusion in this list. It is however the most highly expressed scaffolding protein in this cell line, suggesting that it may have functional significance in ovarian cancer cells.

As expected from the immunofluorescence studies of claudin-4 in OVCAR3 cells (Figure 1), the claudin-4-BioID biotinylated proteins (52 total proteins) were localized to: the nucleus (1 protein; supplementary Table 2A), the Golgi and endoplasmic reticulum (6 proteins; supplementary Table 2A, Figure 4), cytoplasmic transport vesicles (5 proteins; supplementary Table 2B), cell-cell junctions (8 proteins, supplementary Table 2C), the cytoskeleton (8 proteins; supplementary Table 2D) or the plasma membrane (23 proteins including receptors, adhesion molecules, and membrane transporters; supplementary Tables 2E, 2F, 2G). All these proteins are membrane or membrane-associated proteins. These experiments show conclusively that claudin-4 is distributed in all membrane compartments of the cell except perhaps the mitochondria. In the claudin-4 BioID experiment, biotinylation was similar in both the OVCAR3 cells (with large quantities of CLDN4 protein) and the OVCAR8 cells (with barely detectable claudin-4 protein). This finding indicates that localization is not dependent on the presence of endogenous claudin-4.

Because of the orientation of claudin-4 in the membranes, biotinylated membrane proteins must have at least part of their structure on the cytoplasmic side of the membrane compartments where the N-terminus of claudin-4 would be located. Because claudin-4 appears by immunohistochemistry to be heavily represented in the ER and Golgi compartment, we examine data related to these compartments in this text. In addition, claudins are generally thought to be tight junction proteins; we therefore examine the biotinylated proteins associated with cell-cell junctions more closely, finding no clear evidence that claudin-4 acts as a tight junction protein in OVCAR3 cells. Finally, we look at the distribution of a well-studied plasma membrane protein, Notch2, which showed substantial colocalization with CLDN2 in OVCAR3 cells.

**BioID proteins associated with the endoplasmic reticulum (ER) and Golgi apparatus (**Supplementary Table 2A, Figure 4A). Six proteins associated with the ER-GOLGI complex were significantly biotinylated by biotin ligase bound CLDN4. Two prominent Golgi proteins, **GMAP210 (TRIP)** (Infante et al., 1999) and **GOLGB1 (Giantin)** (Linstedt and Hauri, 1993), were biotinylated. These are elongated coiled-coil proteins whose carboxy terminus is anchored to the Golgi membrane. Using immunocytochemistry, both proteins overlapped with claudin-4 (Figures 4B and C). Proteins associated with the trans-Golgi membranes were also biotinylated including **AP1B1** (Anitei et al., 2010), **IGF2R** (Brown et al., 2008), and **CPD** (Thomas et al., 2015). Finally, **YES1** (Zhou et al., 2020), a cytoplasmic non-receptor kinase, shuttles between the Golgi and the plasma membrane and was biotinylated. In conclusion claudin-4 is associated with many proteins in the Golgi compartment.

**Proteins associated with cell-cell junctions,** supplementary Table 2C. Three different types of junctions link epithelial cells to neighboring epithelial cells – tight junctions, adherens junctions, and desmosomes (Figure 5A). The mRNA expression levels for these proteins are available in the TCGA and are shown in Figure 5B. The first five proteins shown in Figure 5B, CLDN4, CLDN3, TJP1 (ZO-1), CDH1, and AHNAK, were not significantly biotinylated in the BioID experiment but are shown here to give a measure of their expression in HGSOC. Both claudin-3 and claudin-4 have been found to be overexpressed in HGSOC in a number of laboratories (Zhang et al., 2018a; Rangel et al., 2003; Choi et al., 2007). TJP1, also known as ZO-1, is an important component of classic tight junctions providing a cytoplasmic anchor for the YV sequences that terminate classic claudins, including claudin-4 and claudin-3 (Nomme et al., 2015). The facts that it was not biotinylated and its low expression in the TCGA led us to the hypothesis that classic tight junctions may not be formed between HGSOC cells.

**LSR** (lipolysis stimulated lipoprotein receptor) is a component of the tricellular junctions as well as being a lipid transporter in the plasma membrane (Masuda et al., 2011). It was prominently biotinylated. **OCLN** is often associated with tight junctions, but it can also be associated with adherens junction proteins (Muller et al., 2005). The junctional protein E-cadherin (CDH1) is heavily associated with cell borders in OVCAR3 cells (Figure 5C) where it likely participates in calcium-dependent cell-cell interactions (Sundfeldt et al., 1997). While CDH1 was not biotinylated in the BioID experiment, its interacting proteins, **CTNND1** (Ishiyama et al., 2010), **DLG1** (Marziali et al., 2019), and **CXADR** (Nilchian et al., 2019) were. The heavy staining of DLG1 in OVCAR3 cells (Figure 5C) is consistent with the hypothesis that adherens junctions may be important in cell-cell interactions of ovarian cancer cells.

Members of the protein families that make up desmosomes (Figure 5A (Green et al., 2019);), the transmembrane cadherin family (desmoglein, **DSG2**, and desmocollin, **DSC2**), the armadillo family protein (plakoglobin, **JUP)** (Aktary et al., 2017), as well as **DLG1**, interacted with claudin-4 in the BioID experiment. JUP is thought to be a biomarker for ovarian cancer (Weiland et al., 2020) as well as being active in the Wnt signaling pathway (Aktary et al., 2017). These findings indicate that claudin-4 is present in or near most of the junctional complexes in OVCAR3 ovarian cancer cells but the lack of interaction with TJP1 (ZO1) and the low expression 0f the mRNA for TJP1 suggest that claudin-4 is not acting as a tight junction protein in these cancer cells.

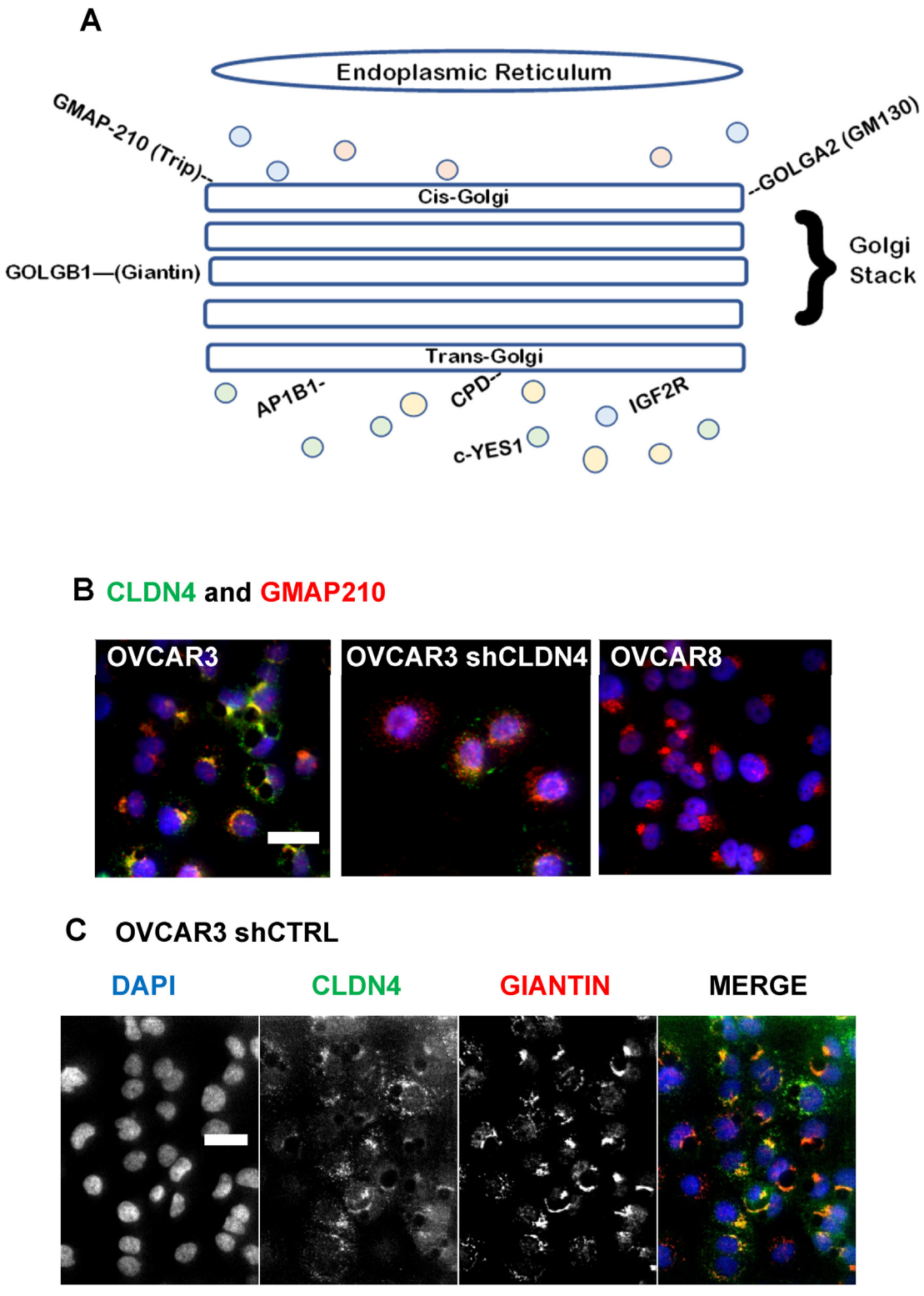


**Figure 4.** ER, Golgi and endosomal proteins identified in the BioID experiment. A. Diagram showing position of Golgi-related proteins. Adapted from (Modica et al., 2017). B. Merged immunocytochemical images of claudin-4 (green), GMAP210—TRIP11 (red) and nuclei (blue) in OVCAR3 shCTRL cells, OVCAR3 shCLDN4 cells and OVCAR 8 cells. Overlapping CLDN4 and GMAP10 appear yellow. C. Images of claudin-4 (green), GOLGB1—Giantin (red) and nuclei (blue) in OVCAR3 shCTRL cells showing overlap (yellow) between the two molecules. Scale bars: 10 μM.

**Proteins associated with the plasma membrane.** Plasma membrane proteins traverse the plasma membrane and interact with elements of external environment of the tumor cells. Supplementary Figure 2 shows the mRNA expression levels of the 23 membrane proteins from the HGSOC TCGA that were identified with claudin-4-BioID. All the biotinylated proteins from OVCAR3 variants are fairly highly expressed in this large ovarian tumor dataset. They fall into three categories: 1) membrane receptors that interact with hormones like IGF2 or EGF or with membrane resident ligands on adjacent cells, 2) adhesion molecules that interact with extracellular matrix proteins, and 3) transporters that

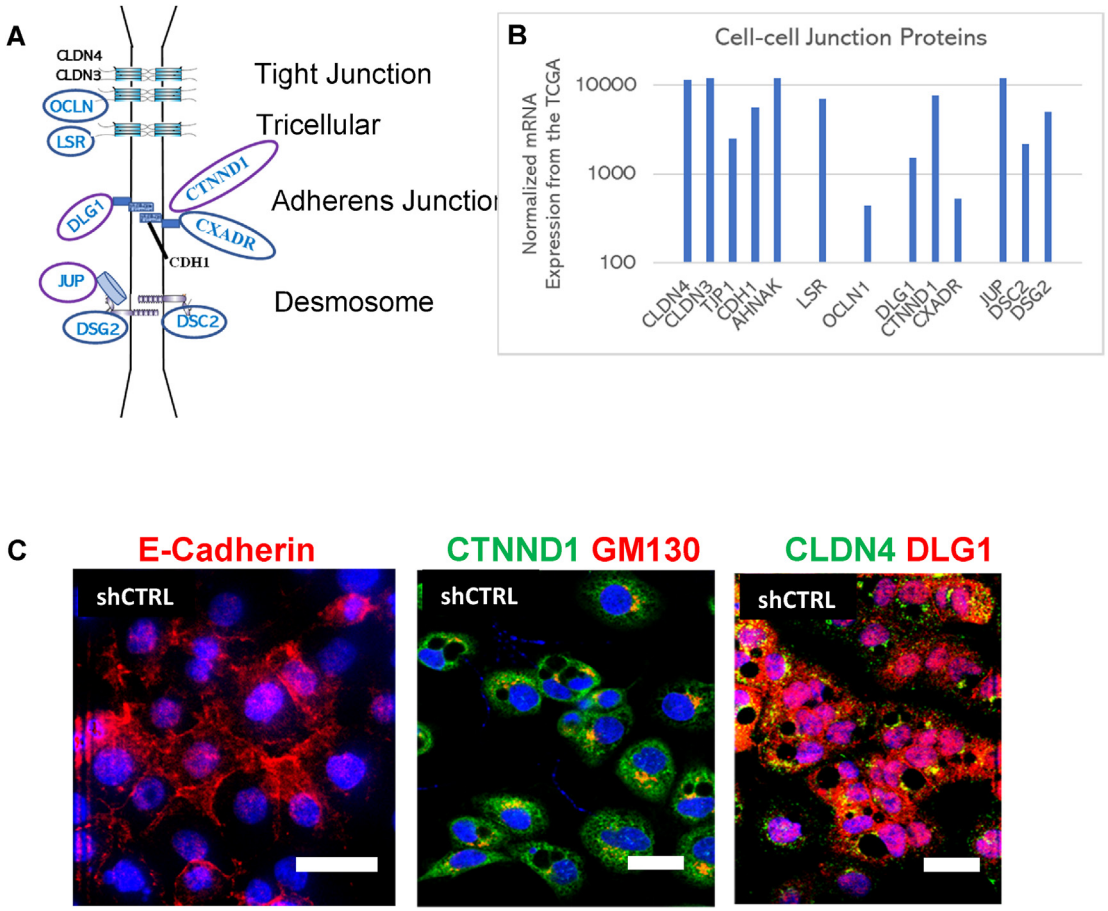


**Figure 5.** Junctional proteins near CLDN4 in OVCAR3 cells. A. Diagram showing proteins associated with the various classes of cell-cell junctions. Circled proteins were labelled in the Bio ID experiment. B. mRNA expression for junctional proteins in the TCGA. Note: Claudin-4, claudin-3, tight junction protein 1 (TJP1), E-cadherin (CDH1), and AHNAK did not fulfill the criteria for interaction with claudin-4 in the BioID experiment but are junction-associated proteins expressed at high levels in HGSOC. Some, like the claudins and AHNAK, are expressed at very high levels. C. Immuno-fluorescence images of E-cadherin, GM130 with CTNND1, and DLG1 with CLDN4 in OVCAR3 cells. Scale bars: 10 μM.

transfer ions and nutrients into the cell. The biotinylation of all these proteins provides strong evidence that claudin-4 is associated with plasma membranes in OVCAR3 cells. Of these molecules we discuss Notch2 here because it overlaps extensively with claudin-4 by immunohistochemistry. Brief summaries of the actions of the other identified plasma membrane proteins are given in Supplementary Tables 2E-G.

**Notch receptor 2.** Co-culture of ovarian cancer cells and endothelial cells induced increased Notch receptors on the surface of the ovarian cells as well as an increase in the Notch ligand Jagged1 on the endothelial cells (Hoarau-Véchot et al., 2019). The authors suggested that Notch2 mediates interactions between ovarian cancer cells and the endothelium. The mRNA for NOTCH2 is the most highly expressed in the TCGA of the biotinylated receptors in HGSOC cells (supplementary Figure 2). In OVCAR3 cells Notch receptor 2 protein was found at the cell border; this is particularly evident in the CLDN4 knockdown cells (Figure 6A). A significant increase in the area occupied by Notch2 was observed in the CLDN4 knockdown cells and about half the area occupied by NOTCH2 overlapped with the CLDN4 area in both shCTRL and shCLDN4 cells (Figure 6B). Since NOTCH2 mRNA is not significantly increased in shCLDN4 cells (unpublished data), this finding suggests that claudin-4 protein localized to the membrane alters the membrane distribution of Notch2 by an unknown mechanism. Interestingly, claudin-4 and Notch2 are colocalized in vesicles surrounding the nuclei of dividing OVCAR3 cells (Figure 6C). High NOTCH2 expression was correlated with worse overall survival in all ovarian cancers (Zhou et al., 2016). Many putative Notch targeting agents are in study with 70 clinical trials registered in 2020 (Moore et al., 2020) suggesting the importance of studies of the interaction of claudin-4 and Notch2.

## 3. Discussion

Claudins are best known as molecules that promote tight junction closure in normal epithelia, interacting with the scaffold protein ZO-1 (TJP1) in complex ways to promote the transepithelial barrier. Claudin-4 is only sporadically found in normal epithelia but is highly expressed in many epithelial cancers including breast (Kolokytha et al., 2014; Szasz et al., 2011), prostate (Landers et al., 2008; Li, 2021), pancreatic (Li, 2021; Torres et al., 2018), bladder (Kuwada et al., 2015), lung (Li, 2021), gastric (Liu and Li, 2020), colorectal (Holczbauer et al., 2013) and ovarian (Hewitt et al., 2006; Hough et al., 2000; Li, 2021). In many of these cancers, although claudin-4 appears to be localized in the membranes, the cellular compartments with which it is associated have not been determined.

**Claudin-4 localization.** About 20% of the total area occupied by claudin-4 in OVCAR3 cells localized with the Golgi-associated protein, GM130 even in cells where claudin-4 was partially knocked down (Table 1). Claudin-4 was also associated with cell borders as well as in distinct cytoplasmic puncta (Figure 1). To localize claudin-4 more precisely, we performed a BioID experiment, transducing both OVCAR3 and OVCAR8 cells with the gene for claudin-4 with the biotin ligase gene attached to the N-terminus. We then determined the identity of biotinylated proteins in cultures of these cell lines. OVCAR8 cells express

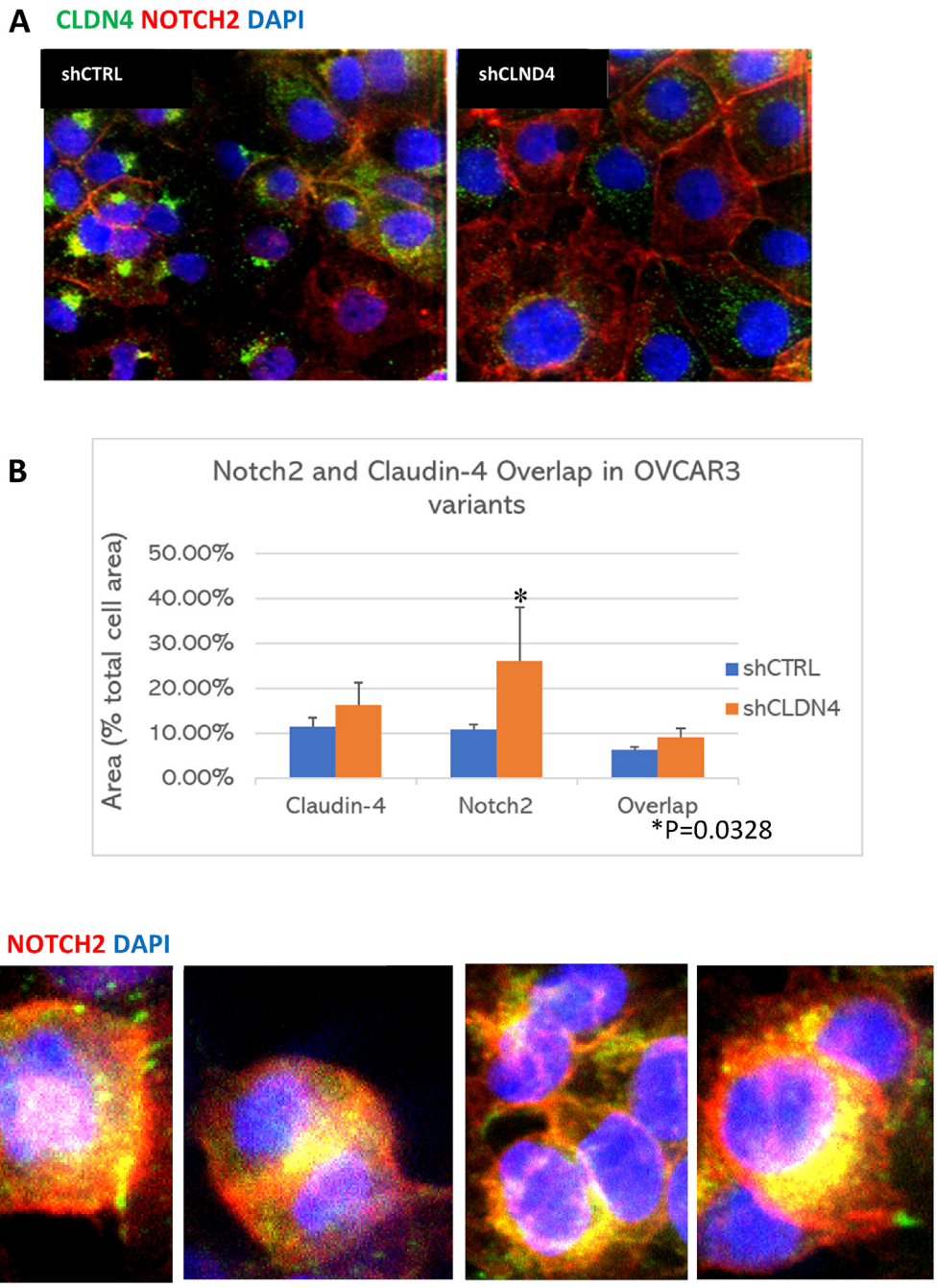


**Figure 6.** Overlap between Notch2 and claudin-4 in. A. Immunohistochemical staining of Notch2 and claudin-4 in OVCAR3 shCNTL and shCLDN4 cells. B. Quantitation of cell area occupied by Notch2 and claudin-4 proteins. Area occupied by Notch2 is significantly increased in shCLDN4 cells ($p = 0.0328$). C. Overlap of NOTCH2 and claudin-4 in vesicles surrounding dividing nuclei in 4 sections from OVCAR3 calls.

CLDN4 mRNA at a level less than 1% of the level in OVCAR3 cells, allowing us to determine the effect of endogenous claudin-4. The BioID experiment produced 52 biotinylated proteins of which one (LEMD) is generally localized to the nuclear membrane; six of these are located in the Golgi and endoplasmic reticulum, five in endosomal vesicles, eight at cell-cell junctions, eight with the cytoskeleton, and 23 are plasma membrane proteins. It appears as if, once synthesized, claudin-4 starts down the pathway from the nucleus to the endoplasmic reticulum and Golgi, to endoplasmic vesicles which carry it to the plasma membrane—portions of which are associated with cell-cell junctions and other portions at other cell borders.

The protein neighbors identified in the BioID analysis of claudin-4 provide insight into the structural architecture of the membranes in OVCAR3 cells. Not only were membrane proteins in all cellular compartments (except the mitochondria) biotinylated, many scaffolding proteins adjacent to the membranes were also biotinylated. Scaffolding proteins are often thought to provide a focus for the clustering of functional proteins. Whether the organization of functional proteins depends on expression of claudin-4 is an important question for future investigation. However, previously published findings relating to claudin-4 expression and activity suggest that it plays an important role in the function of tumor cells. Thus, the fraction of apoptotic ovarian tumor cells is altered by the knockdown of claudin-4 (Breed et al., 2019; Hicks et al., 2016). In addition, claudin-4 appears to affect mitotic progression in OVCAR3 cells, perhaps by interaction with tubulin (Breed et al., 2019).

**Claudin-4 and AHNAK.** It is relevant to discuss AHNAK (Neuroblast differentiation-associated protein, SUSD2), a scaffolding protein highly expressed in OVCAR3 cells; it is often associated with the mesenchymal phenotype in cancers (Sheets et al., 2016). Biotinylation of AHNAK was increased 2.04-fold ($\log_2$ 0.78) in the presence of claudin-4-biotin ligase, too low to meet our cut-off because AHNAK has a high basal level of biotinylation. However, AHNAK may be an important protein in epithelial cancers since it is associated both with EMT (Sheets et al., 2016) and with microvesicle production (Silva et al., 2016). It is referred to as a "giant" protein because of its large size, about 5500 amino acids (Davis et al., 2014). Further, the functional classification of AHNAK as a scaffold protein is supported by the presence of a PDZ domain within its protein structure, which could interact with the YV sequence at the C terminus of claudin-4 (Itoh et al., 1999; Zardab et al., 2022). Could it be that the membrane distribution of claudin-4 in OVCAR3 cells is dependent on the scaffolding function of AHNAK?

**Claudin-4 and solute carriers.** Claudin-4 was found in proximity to several solute carriers, including LAT1 (SLC3A2 and SLC7A5), Na/K ATPase (ATP1A1), and ASCT2 (SLC1A5). The interaction and possible regulatory effect of claudin-4 on these solute carriers is intriguing in the context of metabolism and the tumor microenvironment. For instance, LAT1's role in tryptophan uptake has direct implications in the immune response (Hayashi and Anzai, 2022) and regulation of the aryl hydrocarbon receptor transcription factor (D'Amato et al., 2015), which uses a tryptophan metabolite (kynurenine) to reprogram the transcriptome. Another example is that ASCT2 transports the amino acid glutamine, a critical metabolite for the generation of essential molecules (e.g., glucose) and amino acids. The depletion of glutamine uptake and biosynthesis attenuates the growth of ovarian cancer cells (Furusawa et al., 2018). Thus, there is a significant need to further understand the regulatory function of the claudin-4/ASCT2 interaction.

**Claudin-4 and survival.** High expression of claudin-4 is associated with reduced survival in ovarian cancer patients (Human Protein Atlas). Breed and associates (Breed et al., 2019) found that high expression in OVCAR3 variants reduced the apoptotic response to paclitaxel and that the molecule interacted with tubulin. The response could be restored by treatment of the cells with a claudin-4 targeting peptide. A major question is how claudin-4 produces these effects. We have recently shown that loss of claudin-4 expression in ovarian cancer cells decreases DNA repair capacity and increases the sensitivity to PARP inhibitors (Yamamoto et al., 2019, 2022). Consistently, human tumors with low claudin-4 expression correlate with both higher mutational burden and genomic instability. The connection between these findings and the localization of claudin-4 is currently not clear.

**Other claudins in cancer cells.** Claudin-4 is not the only claudin in ovarian cancer cells (Li, 2021; Rangel et al., 2003). CLDN3 is expressed at a higher average level in ovarian tumors in the TCGA than either CLDN4 or CLDN1, while CLDN6 and CLDN7 are also expressed at significant levels. Claudin-3 was localized throughout the cell in many ovarian cancers although the precise membranes in which it was distributed were not determined (Corsini et al., 2018). An important question is whether claudins-3, 6, 7 are localized in membrane or membrane adjacent compartments in cancer cells. What are the biological actions of all these claudins in epithelial cancer cells?

**Phosphorylated claudin-4.** Phosphorylated claudin-4 is relatively understudied. In OVCAR3 cells, claudin-4 phosphorylated on Y208 was localized to cytoplasmic puncta that also contained non-phosphorylated focal adhesion kinase raising the question of whether phosphorylated claudin-4 is involved in the formation of focal adhesion complexes. Tanaka and colleagues found that claudin-4 was phosphorylated on Y208 by EPHA2, a process that attenuated its interaction with ZO-1 in the tight junctions of MDCK cells (Tanaka et al., 2005). While there is no evidence that phosphorylated claudin-4 interacts with tight junction proteins such as ZO-1 (also known as TJP1) in ovarian cancer cells, it is clear that it is tightly regulated and confined to cytoplasmic puncta in these cells. Phosphorylated claudin-4 appeared to be present at about the same level in cells where CLDN4 is knocked down (shCLDN4 cells) as in control cells (shCTRL; Figure 2B) where total non-phosphorylated claudin-4 is significantly diminished. Whether this finding is the result of a saturation of the phosphorylation mechanism in the control cells, or some other mechanism, remains to be determined.

**Summary and limitations of this study**. The overall aim of this study was to determine the localization of claudin-4 in ovarian cancer cells. In the course of these experiments we found that claudin-4 is localized to most membranes of the cell, that native and phosphorylated claudin-4 did not colocalize, that about 20% of claudin-4 was localized to the Golgi in both normal and claudin-4 knockdown cells, and that claudin-4 continued its Golgi localization in cells where the Golgi is dispersed including dividing cells where it colocalized with both the Golgi marker GM130 and with the plasma membrane receptor Notch2.

One limitation of this study is that neither other types of ovarian cancer cells nor actual ovarian tumors were studied. There do not seem to be studies of the localization of claudins in other types of epithelial cancers; it seems possible that claudins other than claudin-4 may be localized in membrane areas that are not tight junctions. This finding would have important implications for therapeutic agents. For example, claudin-4 has been shown to reduce the response of ovarian cancer cells to paclitaxel (Breed et al., 2019); the mechanism of this action is unknown.

## 4. Star

### 4.1. Methods

**Cell lines and cell culture.** Human derived OVCAR3 and OVCAR8 cells were obtained from the laboratory of Monique Spillman at the University of Colorado and cultured in RPMI-1640 medium (Gibco, Thermo Fisher Scientific) plus 10% heat inactivated fetal bovine serum and penicillin/streptomycin at 37 °C and 5% $CO_2$. Cell lines were authenticated by short tandem repeat profiling at the University of Arizona Genetics Core.

**shRNA knockdown.** OVCAR3 cells were plated $3.2 \times 10^4$ in a 96-well plate and incubated at 37 °C for 24 h. When cells reached 70% confluence, 10 mL of claudin-4 short hairpin RNA (shCLDN4; TRC#: TRCN0000116627, TRCN0000116628, or TRCN0000116631) or control (shCTRL; SHC001, pLK0.1-puro Empty Vector) lentiviral suspension (Sigma-Aldrich MISSION shRNA, University of Colorado Functional Genomics Facility) was added to the cells, which were incubated overnight at 37 °C. Fresh medium was added to remove lentivirus and cells were allowed to recover for 24 h before being treated with 0.5 mg/mL puromycin for selection and expansion of transduced cells. Western blot analysis confirmed the decrease in claudin-4 expression.

**Data from The Cancer Genome Atlas** (TCGA, 2011). The TCGA contains expression values for 20532 mRNAs from 209 ovarian cancer patients. RNA-seq data was downloaded from cbioportal and compiled. The patient values were averaged, and the standard deviation and standard errors of the mean determined.

**Bio ID.** *Constructs* - pTRE2 hyg myc biotin ligase CLDN4 plasmid was a gift from Melvin Anderson at NIH. The myc biotin ligase CLDN4 was excised using Bam HI and Sal I and ligated into a pBABE vector. A control plasmid with a stop codon before CLDN4 was also constructed using site directed mutagenesis. Cells were transduced separately with these plasmids.

*Purification of Biotinylated Proteins.* Method adapted from (Van Itallie et al., 2013). 50uM biotin (Sigma B4639) was added to nine 150mm dishes of 80% confluent cells and incubated 16 h. Cells were washed three times with PBS, scraped into PBS, pelleted, lysed in 5 ml RIPA (1% Triton X-100, 0.5% deoxycholate, 0.2% SDS, 50mM Tris pH 7.5, 150mM NaCl and protease inhibitors), sonicated, incubated on ice for 10 min, sonicated again, and centrifuged for 20 min at 12,000 x g. The supernatant was transferred to microfuge tubes with 500µl prewashed Dynabeads MyOne Streptavidin C1 and incubated at 40 °C for 4 h in an end-over-end mixer. The beads were then washed twice with 2% SDS,

once with 0.1% deoxycholate, 1% Triton X-100, 500mM NaCl, 1mM EDTA, 50mM Hepes pH 7.3, once with 250mM LiCl, 1mM EDTA, 0.5 deoxycholate, 0.5% Triton X-100, 10mm Tris pH 8.0, and twice with 50mM Tris pH 7.5, 50mm NaCl. Proteins were eluted from the beads and mass spectrometry carried out by Monika Dzieciatkowska, PhD, in the University of Colorado School of Medicine Biological Mass Spectrometry Proteomics Core Facility.

The experiment was repeated four times, twice with OVCAR3 cells and twice with OVCAR8 cells. The resulting numerical values for levels of biotinylated proteins were analyzed by the difference between cells receiving the gene for claudin with biotin ligase and claudin alone. Only proteins where the difference between the biotinylated and control was greater than 10 and the $\log_2$ ratio was greater than 1 were selected. The final list and summary data are given in Supplementary Table 1. In most cases, all four experiments met the criteria for selection. In a few cases, only three experiments met the criteria, but these proteins were retained in the list. The final list contained 52 proteins. Sixteen of these proteins had been identified previously in a BioID experiment in MDCK cells examining claudin-4 (asterisks in Supplemental Table 1) (Fredriksson et al., 2015).

**Immunohistochemistry.** Cells grown on Type I collagen (Sigma) coated glass slides were fixed with 10% phosphate buffered formalin (Sigma) at room temperature for 15 min. Slides were washed twice with phosphate buffered saline (PBS), permeabilized with 0.5% Triton X-100 (Sigma) for 5 min at room temperature, washed twice with PBS, blocked with 2% bovine serum albumin (Sigma) for 1 h at room temperature, and then treated with primary antibodies (Supplemental Table 3) overnight at 4 °C. Slides were washed with PBS five times before application of secondary antibodies (dilution 1:100) to the same species as the primary antibodies and conjugated to a fluorescent probe (Jackson Immuno Research) as well as 5 μg/ml 4',6-diamidina-2-phenylindole (DAPI, Sigma) for 45 min at room temperature followed by five washes with PBS. OPDA (20 mg/ml, o-phenylenediamine dihydrochloride (Sigma) in 1M Tris, (pH 8.5 and 10% glycerol) was applied to slides for preservation of fluorescence and slides were coverslip mounted. Imaging was performed in the Advanced Light Microscopy Core part of the Neuro Technology Center at University of Colorado Anschutz Medical Campus supported in part by Rocky Mountain Neurological Disorders Core Grant Number P30 NS048154 and by Diabetes Research Center Grant Number P30 DK116073.

**Quantitation of immunohistochemistry.** Quantitation of the area occupied by a particular-colored stain was carried out using Slidebook software (Intelligent Imaging Innovations Inc., Denver, CO).

**Statistical analysis.** Quantitative data are presented as mean +/- SEM. An unpaired Student t-test was used for statistical comparison between control and treatment groups. A P-value of $<0.05$ was considered significant.

## Declarations

### Author contribution statement

Margaret C. Neville: Conceived and designed the experiments; Performed the experiments; Wrote the paper.

Patricia G. Webb: Conceived and designed the experiments; Performed the experiments; Analyzed and interpreted the data; Contributed reagents, materials, analysis tools or data.

Heidi K. Baumgartner: Conceived and designed the experiments; Performed the experiments; Analyzed and interpreted the data.

Benjamin G. Bitler: Conceived and designed the experiments; Analyzed and interpreted the data; Wrote the paper.

### Funding statement

Benjamin G. Bitler was supported by Department of Defense, USA [OC170228, OC200302, OC200225], American Cancer Society [RSG-19-129-01-DDC], Division of Cancer Prevention, National Cancer Institute [R37CA261987].

This work was supported by National Institute of Neurological Disorders and Stroke [P30 NS048154], Diabetes Research Center [P30 DK116073].

### Data availability statement

Data included in article/supp. material/referenced in article.

### Declaration of interest's statement

The authors declare no conflict of interest.

### Acknowledgements

We acknowledge philanthropic contributions from Kay L. Dunton Endowed Memorial Professorship in Ovarian Cancer Research, the McClintock-Addlesperger Family, Karen M. Jennison, Don and Arlene Mohler Johnson Family, Michael Intagliata, Duane and Denise Suess, Mary Normandin, and Donald Engelstad. This work was supported by The Department of Defense (Bitler, OC170228, OC200302, OC200225), The American Cancer Society (Bitler, RSG-19-129-01-DDC), NIH/NCI (Bitler, R37CA261987). The imaging experiments were performed in the Advanced Light Microscopy Core part of Neurotechnology Center at University of Colorado Anschutz Medical Campus supported in part by Rocky Mountain Neurological Disorders Core Grant Number P30 NS048154 and by Diabetes Research Center Grant Number P30 DK116073. Contents of this paper are the authors' sole responsibility and do not necessarily represent the official views of our sponsors. We thank Elizabeth Woodruff and Fabian Romero Villagomez for critical reading of the manuscript.

### Additional information

Supplementary content related to this article has been published online at https://doi.org/10.1016/j.heliyon.2022.e10862.

## References

ACS, 2022. Key Statistics for Ovarian Cancer [Online]. Available: https://www.cancer.org/cancer/ovarian-cancer/about/key-statistics.html [Accessed].

Aktary, Z., Alaee, M., Pasdar, M., 2017. Beyond cell-cell adhesion: plakoglobin and the regulation of tumorigenesis and metastasis. Oncotarget 8, 32270–32291.

Anitei, M., Stange, C., Parshina, I., Baust, T., Schenck, A., Raposo, G., Kirchhausen, T., Hoflack, B., 2010. Protein complexes containing CYFIP/Sra/PIR121 coordinate Arf1 and Rac1 signalling during clathrin-AP-1-coated carrier biogenesis at the TGN. Nat. Cell Biol. 12, 330–340.

Baumgartner, H.K., Beeman, N., Hodges, R.S., Neville, M.C., 2011. A d-peptide analog of the second extracellular loop of claudin-3 and -4 leads to misocalized claudin and cellular apoptosis in mammary epithelial cells. Chem. Biol. Drug Des. 77, 124–136.

Baumgartner, H.K., Rudolph, M.C., Ramanathan, P., Burns, V., Webb, P., Bitler, B.G., Stein, T., Kobayashi, K., Neville, M.C., 2017. Developmental expression of claudins in the mammary gland. J. Mammary Gland Biol. Neoplasia 22, 141–157.

Breed, C., Hicks, D.A., Webb, P.G., Galimanis, C.E., Bitler, B.G., Behbakht, K., Baumgartner, H.K., 2019. Ovarian tumor cell expression of claudin-4 reduces apoptotic response to paclitaxel. Mol. Cancer Res. 17, 741–750.

Brown, J., Delaine, C., Zaccheo, O.J., Siebold, C., Gilbert, R.J., Van Boxel, G., Denley, A., Wallace, J.C., Hassan, A.B., Forbes, B.E., Jones, E.Y., 2008. Structure and functional analysis of the IGF-II/IGF2R interaction. EMBO J. 27, 265–276.

Choi, Y.L., Kim, J., Kwon, M.J., Choi, J.S., Kim, T.J., Bae, D.S., Koh, S.S., In, Y.H., Park, Y.W., Kim, S.H., Ahn, G., Shin, Y.K., 2007. Expression profile of tight junction protein claudin 3 and claudin 4 in ovarian serous adenocarcinoma with prognostic correlation. Histol. Histopathol. 22, 1185–1195.

Colanzi, A., Grimaldi, G., Catara, G., Valente, C., Cericola, C., Liberali, P., Ronci, M., Lalioti, V.S., Bruno, A., Beccari, A.R., Urbani, A., De Flora, A., Nardini, M., Bolognesi, M., Luini, A., Corda, D., 2013. Molecular mechanism and functional role of brefeldin A-mediated ADP-ribosylation of CtBP1/BARS. Proc. Natl. Acad. Sci. U. S. A 110, 9794–9799.

Corsini, M., Ravaggi, A., Odicino, F., Santin, A.D., Ravelli, C., Presta, M., Romani, C., Mitola, S., 2018. Claudin3 is localized outside the tight junctions in human carcinomas. Oncotarget 9, 18446–18453.

D'amato, N.C., Rogers, T.J., Gordon, M.A., Greene, L.I., Cochrane, D.R., Spoelstra, N.S., Nemkov, T.G., D'Alessandro, A., Hansen, K.C., Richer, J.K., 2015. A TDO2-AhR

signaling axis facilitates anoikis resistance and metastasis in triple-negative breast cancer. Cancer Res. 75, 4651–4664.
Davis, T.A., Loos, B., Engelbrecht, A.M., 2014. AHNAK: the giant jack of all trades. Cell. Signal. 26, 2683–2693.
Fredriksson, K., Van Itallie, C.M., Aponte, A., Gucek, M., Tietgens, A.J., Anderson, J.M., 2015. Proteomic analysis of proteins surrounding occludin and claudin-4 reveals their proximity to signaling and trafficking networks. PLoS One 10, e0117074.
Fujiwara-Tani, R., Sasaki, T., Luo, Y., Goto, K., Kawahara, I., Nishiguchi, Y., Kishi, S., Mori, S., Ohmori, H., Kondoh, M., Kuniyasu, H., 2018. Anti-claudin-4 extracellular domain antibody enhances the antitumoral effects of chemotherapeutic and antibody drugs in colorectal cancer. Oncotarget 9, 37367–37378.
Furusawa, A., Miyamoto, M., Takano, M., Tsuda, H., Song, Y.S., Aoki, D., Miyasaka, N., Inazawa, J., Inoue, J., 2018. Ovarian cancer therapeutic potential of glutamine depletion based on GS expression. Carcinogenesis 39, 758–766.
Gong, Y., Hou, J., 2017. Claudins in barrier and transport function-the kidney. Pflueg. Arch. Eur. J. Physiol. 469, 105–113.
Green, K.J., Jai Ganesh, A., Broussard, J.A., 2019. Desmosomes: essential contributors to an integrated intercellular junction network. F1000Res 8.
Hayashi, K., Anzai, N., 2022. L-type amino acid transporter 1 as a target for inflammatory disease and cancer immunotherapy. J. Pharmacol. Sci. 148, 31–40.
Hewitt, K.J., Agarwal, R., Morin, P.J., 2006. The claudin gene family: expression in normal and neoplastic tissues. BMC Cancer 6, 186.
Hicks, D.A., Galimanis, C.E., Webb, P.G., Spillman, M.A., Behbakht, K., Neville, M.C., Baumgartner, H.K., 2016. Claudin-4 activity in ovarian tumor cell apoptosis resistance and migration. BMC Cancer 16, 788.
Hoarau-vechot, J., Touboul, C., Halabi, N., Blot-Dupin, M., Lis, R., Abi Khalil, C., Rafii, S., Rafii, A., Pasquier, J., 2019. Akt-activated endothelium promotes ovarian cancer proliferation through notch activation. J. Transl. Med. 17, 194.
Holczbauer, A., Gyongyosi, B., Lotz, G., Szijarto, A., Kupcsulik, P., Schaff, Z., Kiss, A., 2013. Distinct claudin expression profiles of hepatocellular carcinoma and metastatic colorectal and pancreatic carcinomas. J. Histochem. Cytochem. 61, 294–305.
Hough, C.D., Sherman-Baust, C.A., Pizer, E.S., Montz, F.J., Im, D.D., Rosenshein, N.B., Cho, K.R., Riggins, G.J., Morin, P.J., 2000. Large-scale serial analysis of gene expression reveals genes differentially expressed in ovarian cancer. Cancer Res. 60, 6281–6287.
Infante, C., Ramos-Morales, F., Fedriani, C., Bornens, M., Rios, R.M., 1999. GMAP-210, A cis-Golgi network-associated protein, is a minus end microtubule-binding protein. J. Cell Biol. 145, 83–98.
Ishiyama, N., Lee, S.H., Liu, S., Li, G.Y., Smith, M.J., Reichardt, L.F., Ikura, M., 2010. Dynamic and static interactions between p120 catenin and E-cadherin regulate the stability of cell-cell adhesion. Cell 141, 117–128.
Itoh, M., Furuse, M., Morita, K., Kubota, K., Saitou, M., Tsukita, S., 1999. Direct binding of three tight junction-associated MAGUKs, ZO-1, ZO-2, ZO-3 with the COOH termini of claudins. J. Cell Biol. 147, 1351–1363.
Kolokytha, P., Yiannou, P., Keramopoulos, D., Kolokythas, A., Nonni, A., Patsouris, E., Pavlakis, K., 2014. Claudin-3 and claudin-4: distinct prognostic significance in triple-negative and luminal breast cancer. Appl. Immunohistochem. Mol. Morphol. 22, 125–131.
Kuwada, M., Chihara, Y., Luo, Y., Li, X., Nishiguchi, Y., Fujiwara, R., Sasaki, T., Fujii, K., Ohmori, H., Fujimoto, K., Kondoh, M., Kuniyasu, H., 2015. Pro-chemotherapeutic effects of antibody against extracellular domain of claudin-4 in bladder cancer. Cancer Lett. 369, 212–221.
Landers, K.A., Samaratunga, H., Teng, L., Buck, M., Burger, M.J., Scells, B., Lavin, M.F., Gardiner, R.A., 2008. Identification of claudin-4 as a marker highly overexpressed in both primary and metastatic prostate cancer. Br. J. Cancer 99, 491–501.
Li, J., 2021. Dysregulated expression of claudins in cancer. Oncol. Lett. 22, 641.
Linstedt, A.D., Hauri, H.P., 1993. Giantin, a novel conserved Golgi membrane protein containing a cytoplasmic domain of at least 350 kDa. Mol. Biol. Cell 4, 679–693.
Liu, W., Li, M., 2020. The role of claudin-4 in the development of gastric cancer. Scand. J. Gastroenterol. 55, 1072–1078.
Martin de la fuente, L., Malander, S., Hartman, L., Jonsson, J.M., Ebbesson, A., Nilbert, M., Masback, A., Hedenfalk, I., 2018. Claudin-4 expression is associated with survival in ovarian cancer but not with chemotherapy response. Int. J. Gynecol. Pathol. 37, 101–109.
Marziali, F., Dizanzo, M.P., Cavatorta, A.L., Gardiol, D., 2019. Differential expression of DLG1 as a common trait in different human diseases: an encouraging issue in molecular pathology. Biol. Chem. 400, 699–710.
Masuda, S., Oda, Y., Sasaki, H., Ikenouchi, J., Higashi, T., Akashi, M., Nishi, E., Furuse, M., 2011. LSR defines cell corners for tricellular tight junction formation in epithelial cells. J. Cell Sci. 124, 548–555.
Modica, G., Skorobogata, O., Sauvageau, E., Vissa, A., Yip, C.M., Kim, P.K., Wurtele, H., Lefrancois, S., 2017. Rab7 palmitoylation is required for efficient endosome-to-TGN trafficking. J. Cell Sci. 130, 2579–2590.
Moore, G., Annett, S., Mcclements, L., Robson, T., 2020. Top notch targeting strategies in cancer: a detailed overview of recent insights and current perspectives. Cells 9.
Muller, S.L., Portwich, M., Schmidt, A., Utepbergenov, D.I., Huber, O., Blasig, I.E., Krause, G., 2005. The tight junction protein occludin and the adherens junction protein alpha-catenin share a common interaction mechanism with ZO-1. J. Biol. Chem. 280, 3747–3756.
Nilchian, A., Johansson, J., Ghalali, A., Asanin, S.T., Santiago, A., Rosencrantz, O., Sollerbrant, K., Vincent, C.T., Sund, M., Stenius, U., Fuxe, J., 2019. CXADR-mediated formation of an AKT inhibitory signalosome at tight junctions controls epithelial–mesenchymal plasticity in breast cancer. Cancer Res. 79, 47.
Nomme, J., Antanasijevic, A., Caffrey, M., Van Itallie, C.M., Anderson, J.M., Fanning, A.S., Lavie, A., 2015. Structural basis of a key factor regulating the affinity between the zonula occludens first PDZ domain and claudins. J. Biol. Chem. 290, 16595–16606.
Petrosyan, A., 2015. Onco-golgi: is fragmentation a gate to cancer progression? Biochem. Mol. Biol. J. 1.
Piontek, J., Krug, S.M., Protze, J., Krause, G., Fromm, M., 2020. Molecular architecture and assembly of the tight junction backbone. Biochim. Biophys. Acta Biomembr. 1862, 183279.
Rangel, L.B., Agarwal, R., D'Souza, T., Pizer, E.S., Alo, P.L., Lancaster, W.D., Gregoire, L., Schwartz, D.R., Cho, K.R., Morin, P.J., 2003. Tight junction proteins claudin-3 and claudin-4 are frequently overexpressed in ovarian cancer but not in ovarian cystadenomas. Clin. Cancer Res. 9, 2567–2575.
Schlingmann, B., Molina, S.A., Koval, M., 2015. Claudins: gatekeepers of lung epithelial function. Semin. Cell Dev. Biol. 42, 47–57.
Schumann, M., Kamel, S., Pahlitzsch, M.-L., Lebenheim, L., May, C., Krauss, M., Hummel, M., Daum, S., Fromm, M., Schulzke, J.-D., 2012. Defective tight junctions in refractory celiac disease. Ann. N. Y. Acad. Sci. 1258, 43–51.
Sheets, J.N., Iwanicki, M., Liu, J.F., Howitt, B.E., Hirsch, M.S., Gubbels, J.A., Drapkin, R., Egland, K.A., 2016. SUSD2 expression in high-grade serous ovarian cancer correlates with increased patient survival and defective mesothelial clearance. Oncogenesis 5, e264.
Silva, T.A., Smuczek, B., Valadão, I.C., Dzik, L.M., Iglesia, R.P., Cruz, M.C., Zelanis, A., De Siqueira, A.S., Serrano, S.M., Goldberg, G.S., Jaeger, R.G., Freitas, V.M., 2016. AHNAK enables mammary carcinoma cells to produce extracellular vesicles that increase neighboring fibroblast cell motility. Oncotarget 7, 49998–50016.
Soini, Y., TommolaOMMOLA, S., Helin, H., Martikainen, P., 2006. Claudins 1, 3, 4 and 5 in gastric carcinoma, loss of claudin expression associates with the diffuse subtype. Virchows Arch. 448, 52–58.
Sundfeldt, K., Piontkewitz, Y., Ivarsson, K., Nilsson, O., Hellberg, P., Brännström, M., Janson, P.O., Enerback, S., Hedin, L., 1997. E-cadherin expression in human epithelial ovarian cancer and normal ovary. Int. J. Cancer 74, 275–280.
Szasz, A.M., Nemeth, Z., Gyorffy, B., Micsinai, M., Krenacs, T., Baranyai, Z., Harsanyi, L., Kiss, A., Schaff, Z., Tokes, A.M., Kulka, J., 2011. Identification of a claudin-4 and E-cadherin score to predict prognosis in breast cancer. Cancer Sci. 102, 2248–2254.
Tanaka, M., Kamata, R., Sakai, R., 2005. EphA2 phosphorylates the cytoplasmic tail of Claudin-4 and mediates paracellular permeability. J. Biol. Chem. 280, 42375–42382.
TCGA, 2011. Integrated genomic analyses of ovarian carcinoma. Nature 474, 609–615.
Thomas, L.N., Merrimen, J., Bell, D.G., Rendon, R., Too, C.K.L., 2015. Prolactin- and testosterone-induced carboxypeptidase-D correlates with increased nitrotyrosines and Ki67 in prostate cancer. Prostate 75, 1726–1736.
Torres, J.B., Knight, J.C., Mosley, M.J., Kersemans, V., Koustoulidou, S., Allen, D., Kinchesh, P., Smart, S., Cornelissen, B., 2018. Imaging of claudin-4 in pancreatic ductal adenocarcinoma using a radiolabelled anti-claudin-4 monoclonal antibody. Mol. Imag. Biol. 20, 292–299.
Uthayanan, L., El-Bahrawy, M., 2022. Potential roles of claudin-3 and claudin-4 in ovarian cancer management. J. Egypt. Natl. Cancer Inst. 34, 24.
Van Itallie, C.M., Anderson, J.M., 2018. Phosphorylation of tight junction transmembrane proteins: many sites, much to do. Tissue Barriers 6, e1382671.
Van Itallie, C.M., Aponte, A., Tietgens, A.J., Gucek, M., Fredriksson, K., Anderson, J.M., 2013. The N and C termini of ZO-1 are surrounded by distinct proteins and functional protein networks. J. Biol. Chem. 288, 13775–13788.
Weiland, F., Lokman, N.A., Klingler-Hoffmann, M., Jobling, T., Stephens, A.N., Sundfeldt, K., Hoffmann, P., Oehler, M.K., 2020. Ovarian blood sampling identifies junction plakoglobin as a novel biomarker of early ovarian cancer. Front. Oncol. 10, 1767.
Yamamoto, T.M., Mcmellen, A., Watson, Z.L., Aguilera, J., Ferguson, R., Nurmemmedov, E., Thakar, T., Moldovan, G.L., Kim, H., Cittelly, D.M., Joglar, A.M., Brennecke, E.P., Wilson, H., Behbakht, K., Sikora, M.J., Bitler, B.G., 2019. Activation of Wnt signaling promotes olaparib resistant ovarian cancer. Mol. Carcinog. 58, 1770–1782.
Yamamoto, T.M., Webb, P.G., Davis, D.M., Baumgartner, H.K., Woodruff, E.R., Guntupalli, S.R., Neville, M., Behbakht, K., Bitler, B.G., 2022. Loss of claudin-4 reduces DNA damage repair and increases sensitivity to PARP inhibitors. Mol. Cancer Therapeut. 21, 647–657.
Yoshida, H., Sumi, T., Zhi, X., Yasui, T., Honda, K., Ishiko, O., 2011. Claudin-4: a potential therapeutic target in chemotherapy-resistant ovarian cancer. Anticancer Res. 31, 1271–1277.
Zardab, M., Stasinos, K., Grose, R.P., Kocher, H.M., 2022. The Obscure Potential of AHNAK2, 14. Cancers, Basel).
Zhang, L., Feng, T., Spicer, L.J., 2018a. The role of tight junction proteins in ovarian follicular development and ovarian cancer. Reproduction 155, R183–r198.
Zhang, X.-M., Huang, Y., Zhang, K., Qu, L.-H., Cong, X., Su, J.-Z., Wu, L.-L., Yu, G.-Y., Zhang, Y., 2018b. Expression patterns of tight junction proteins in porcine major salivary glands: a comparison study with human and murine glands. J. Anat. 233, 167–176.
Zhou, X., Teng, L., Wang, M., 2016. Distinct prognostic values of four-Notch-receptor mRNA expression in ovarian cancer. Tumour. Biol. 37, 6979–6985.
Zhou, Y., Chen, P., Huang, Q., Wan, T., Jiang, Y., Jiang, S., Yan, S., Zheng, M., 2020. Overexpression of YES1 is associated with favorable prognosis and increased platinum-sensitivity in patients with epithelial ovarian cancer. Histol. Histopathol. 35, 721–728.